A FORCE AND THERMAL SENSING SKIN FOR ROBOTS IN HUMAN ENVIRONMENTS

A Thesis
Presented to
The Academic Faculty

By

Joshua C. Wade

In Partial Fulfillment
of the Requirements for the Degree
Master of Science in the
School of Mechanical Engineering

Georgia Institute of Technology

May 2017

A FORCE AND THERMAL SENSING SKIN FOR ROBOTS IN HUMAN ENVIRONMENTS

Approved by:

Dr. Charlie Kemp, Co-Advisor
School of Biomedical Engineering
Georgia Institute of Technology

Dr. Lena Ting, Co-Advisor
School of Mechanical Engineering
Georgia Institute of Technology

Dr. Jun Ueda
School of Mechanical Engineering
Georgia Institute of Technology

Date Approved: April 21, 2017

ACKNOWLEDGEMENTS

I thank Dr. Charlie Kemp and Tapo Bhattacharjee for serving as my mentors during my time at the Healthcare Robotics Lab. I thank Dr. Ting for serving as my co-adviser and for serving on my thesis reading committee. I thank Dr. Jun Ueda for serving on my thesis reading committee. I thank Ryan Williams for his technical insight. Most of all, I am grateful for the love and support of my family who always encouraged me to dream big.

TABLE OF CONTENTS

LIST OF TABLES

LIST OF FIGURES

SUMMARY

Working together, heated and unheated temperature sensors can recognize contact with different materials and contact with the human body. As such, distributing these sensors across a robot's body could be beneficial for operation in human environments. We present a stretchable fabric-based skin with force and thermal sensors that is suitable for covering areas of a robot's body, including curved surfaces. It also adds a layer of compliance that conforms to manipulated objects, improving thermal sensing. Our design addresses thermal sensing challenges, such as the time to heat the sensors, the efficiency of sensing, and the distribution of sensors across the skin. It incorporates small self-heated temperature sensors on the surface of the skin that directly make contact with objects, improving the sensors' response times. Our approach seeks to fully cover the robot's body with large force sensing taxels, but treats temperature sensors as small, point-like sensors sparsely distributed across the skin. We present a mathematical model to help predict how many of these point-like temperature sensors should be used in order to increase the likelihood of them making contact with an object. To evaluate our design, we conducted tests in which a robot arm used a cylindrical end effector covered with skin to slide objects and press on objects made from four different materials. After assessing the safety of our design, we also had the robot make contact with the forearms and clothed shoulders of 10 human participants. With 2.0 s of contact, the actively-heated temperature sensors enabled binary classification accuracy over 90% for the majority of material pairs. The system could more rapidly distinguish between materials with large differences in their thermal effusivities (e.g., 90% accuracy for pine wood vs. aluminum with 0.5 s of contact). For discrimination between humans vs. the four materials, the skin's force and thermal sensing modalities achieved 93% classification accuracy with 0.5 s of contact. Overall, our results suggest that our skin design could enable robots to recognize contact with distinct task-relevant materials and humans while performing manipulation tasks in human environments.

CHAPTER 1
INTRODUCTION

Covering the surface of a robot's body with multimodal tactile sensors could be advantageous for numerous applications where robots work in close proximity to people. For example, whole-arm force sensing can improve a robot's ability to reach locations in clutter [1], and robots can provide better assistance with some tasks if they're allowed to make contact between their arms and people [2]. More generally, a robot could use multimodal tactile sensors to gather more information about the world when contact occurs with people or objects in its surroundings.

While distributing force sensors across the bodies of robots has been widely explored, other modalities for tactile sensing over larger areas have received less attention. We previously conducted research on thermal sensing using data collected by handheld devices operated by humans [3]. Although we did not conduct tests with a robot, our work suggested that robots that operate in indoor human environments, such as homes, offices, and healthcare facilities, might benefit from thermal tactile sensing that uses actively heated temperature sensors (active thermal sensors) together with unheated temperature sensors (passive thermal sensors). Active thermal sensors are useful for recognizing materials at the ambient temperature, due to heat transferring from the heated sensor to the material. Passive thermal sensors have advantages for recognizing contact with humans indoors, since heat from the human body transfers to the passive thermal sensor, which is near room temperature.

Active thermal sensors can recognize contact with different materials due to variations in how heat transfers from the sensor to the material. Notably, the temperature of the active thermal sensor drops more rapidly and achieves a lower steady state temperature when it makes contact with a material that has a higher thermal effusivity. Passive thermal sensors

can recognize contact with people due to the heat generated by the human body. The temperature of a passive thermal sensor in a typical climate controlled indoor environment will start to rise once in contact with a person's body and, in many cases, will do so even when in contact with clothing worn by a person. In contrast, the temperature of a passive thermal sensor will tend to remain constant when in contact with materials at the ambient temperature [3].

In this thesis, we present our design of a multimodal fabric-based tactile sensing skin for robots in human environments. The skin integrates stretchable fabric-based force sensors and discrete temperature sensors in the form of thermistors, which have an electrical resistance that varies with temperature. Our design uses small off-the-shelf thermistors with a low time constant to improve the speed with which inferences can be made. The skin's stretchable fabric-based design enables it to cover curved surfaces on a robot and, possibly, articulated joints [4]. In addition, the layers of fabric result in the skin being compliant, which could be beneficial for operating around people and enables the skin to conform to manipulated objects. This improves contact between the temperature sensors and manipulated objects, thereby improving thermal sensing.

In addition, we present a characterization and evaluation of the skin, as well as a general mathematical model for selecting the number of thermal sensors to cover the skin. This model provides an analysis tool to help designers increase the chance of contact between the thermal sensors and manipulated objects.

To evaluate our skin design, we used a real robot performing controlled manipulation tasks in a human environment. We covered a cylindrical end effector with our skin prototype and used the end effector with a Meka M1 Mobile Manipulator. The robot performed two manipulation tasks with four materials: pressing an object for 2.0 s and sliding an object across a table. We also had the robot press the bare forearm and clothed shoulder of 10 human participants. We used the skin's force sensors to detect the start of contact and used support vector machines (SVMs) to recognize the touched object based on the sensor data

in multiclass and binary classification problems. We used the skin's active thermal sensors to distinguish between material samples and the skin's force, active and passive thermal sensors to recognize contact with the human body.

We based our study of binary classification on the notion that many material recognition problems that a robot could encounter while assisting people could involve binary classification [3]. Tasks can sometimes be considered to involve a tactile foreground, such as an object to be grasped, and a tactile background, such as the surface on which the object rests. For example, if a robot were to reposition a person's limb as he or she sits in a wheelchair, it might use tactile sensing to distinguish the person's body from the metal wheelchair. Similarly, while navigating within a human environment, distinguishing between contact with a human versus contact with the surrounding environment could be used to inform a robot's behavior.

Chapter 2 discusses related work focused on force and thermal tactile sensing for robots. Chapter 3 describes the development of the skin and construction of the prototype that covers a robot's end effector. In Chapter 4, we present a geometric model to inform the distribution of thermal sensors across the skin. We also characterize the noise level of the thermal sensors, the speed of response of the active thermal sensors and perform a safety analysis of the active thermal sensors for use in human environments. Chapter 5 details our evaluation of the skin and Chapter 6 summarizes the results of our evaluation and discusses capabilities and limitation of the system. Chapter 7 presents our conclusions.

CHAPTER 2
RELATED WORK

Tactile sensors measuring force or pressure have been used on many robotic platforms and are often implemented as arrays or skins [5], [6], [7], [8]. In this work we define robotic skin as a sensorized covering for a 3 dimensional robot as opposed to a two dimensional sensor array that can only cover a flat surface. In some cases skins are made of stretchable fabrics to allow the skin to cover surfaces with complex curvature [9], [10]. As discussed in our previous work [3], [11], many robotic systems also benefit from thermal tactile sensors including active thermal sensors for discriminating between materials based on heat transfer or passive thermal sensors for identifying objects at different temperatures. For active thermal sensing, some researchers have used arrays of temperature sensors combined with a common resistive heating element to realize a thermal sensing array as seen in [12] and [13]. While most researchers use thermistors or resistance temperature detectors (RTDs) for temperature sensing, other devices including Peltier effect sensors [14], pyrometers [15] and more recently pectin films [16] have been used.

Combining force and thermal sensing into a multimodal sensor remains an active area of research. In some cases, researchers have used compact multimodal sensors to cover a small area such as a robot fingertip, while other studies have focused on realizing multimodal sensing arrays or skins to cover larger areas of the robot.

2.1 Small Area Force and Thermal Sensors

In contrast to the devices in this section, which are designed to provide sensation over a relatively small area, our skin design provides multimodal sensation over a larger area ($60\,\mathrm{cm}^2$) and can be further scaled-up.

The Syntouch BioTAC is a multimodal robotic fingertip sensor that has been widely

used in robotics applications for material and object identification [17], [18], [19], [20], [21]. The BioTAC features 19 impedance sensing electrodes for force estimation (both direction and magnitude) and a single thermistor combined with inherent heat generation in the sensor's electrical hardware for active thermal sensing. One drawback of the Syntouch BioTAC, is that the thermistor takes significant time to heat up and to transfer heat to objects, in part because of the placement of the thermistor in the interior of the finger and the lack of controlled heating specifically for the thermistor. In contrast, our design places the thermistors on the exterior of the surface and directly heats the thermistors in a controlled manner.

Taddeucci et al. presented a robot fingertip sensor featuring 64 force-sensing taxels made of peizo-resistive silk screen ink and a single heater and thermistor for active thermal sensing [22]. Caldwell et al. developed a similar fingertip sensor using a fiber optic force sensor and a Peltier effect sensor [14]. Yuji et al. constructed a 2x2 array of resistive force and passive thermal sensors using pressure conductive rubber [23].

Engel et al. constructed a high resolution skin designed to cover a robot's fingertip with multiple force and active and passive thermal sensors on a flexible printed circuit board (FPCB). They used discrete heating elements to locally warm certain temperature sensors while leaving other temperature sensors unheated for passive thermal sensing [24], [25]. This method is advantageous for combined active and passive thermal sensing compared to using a common heat source, because heating the entire device may cause heat to flow into the passive thermal sensors and bias their temperature measurements.

While their use of both active and passive thermal sensing is related to our approach, our use of stretchable fabric could allow our skin to cover shapes with more complex curvature, which addresses one of the limitations of the device developed by Engel et al. [24]. Additionally, we use a geometric model to design the arrangement of sparsely-distributed thermal sensors, which reduces the required number of the analog channels and may improve the scalability of our system for covering larger areas.

2.2 Large Area Force and Thermal Sensors

To provide multimodal sensation over a larger area, researchers have used multimodal tactile sensing arrays or skins with multiple force and thermal sensors. Examples include [26], [27], [28], where arrays of force and temperature sensors were realized with an FPCB or similar polyimide substrate. While this material provides a durable substrate for sensor mounting and can flex to cover surfaces with single curvature such as cylinders, continuous FPCB sheets may not have the requisite flexibility and stretchability to cover more complex 3D shapes according to [24].

Mittendorfer et al. developed small rigid hexagonal printed circuit boards (PCBs) equipped with sensors for force, temperature, acceleration, and proximity and demonstrated how multiple units can be connected together via FPCB strips to form a skin. Similar to the BioTac sensor, their design used inherent heat generation from the electrical hardware to generate heat for active thermal sensing [29], [30], [31]. To cover surfaces with more complex curvature, Maiolino et al. realized a capacitive force sensing skin using interconnected FPCB sensing modules covered by a common layer dielectric made of 3D air mesh fabric. Each triangular module included 2 passive thermal sensors for thermal compensation of the 10 capacitive force sensors [28]. Similarly Castelli et al. built an array of capacitive force sensors with integrated passive thermal sensors [32].

In contrast to these devices with only one type of thermal sensing (active or passive), our design incorporates both active and passive thermal sensing in a fabric-based design. We achieve this with two groups of self-heated thermistors that can be independently heated to software-specified temperatures using feedback control. Moreover, we show that the thermistors can be safely heated to temperatures well-above the ambient temperature and likely above temperatures that could be reasonably obtained via inherent heat generation. In this work, we use this capability for simultaneous active and passive thermal sensing, but all the sensors could be active with 2 independent temperatures or all passive. Our skin is made

of stretchable fabric similar to [9] and [10]. This use of stretchable fabric could potentially allow the skin to cover surfaces with more complex curvature and time-varying geometry on a robot, such as articulated joints [4].

Our approach is also distinctive in that we prioritize coverage for the force sensors in our skin to ensure contact will be detected, but use sparse temperature sensors that are very small compared to the area of the skin. As our model and experiments support, sparse point-like sensors can usefully make contact with low-curvature objects of sufficient size. This presents the opportunity to scale up the skin more easily for some applications with large, low-resolution force sensing areas covering the full skin and small, sparse temperature sensors providing additional information when they are in contact.

2.3 Evaluation of Force and Thermal Sensors with Robots

A number of studies have used force and thermal sensor feedback from the BioTAC sensor to aid in object recognition. Xu et al. attached the BioTAC to the finger of a robotic hand and had the robot touch and identify various material samples using multimodal sensor feedback [17]. Chu et al. attached two BioTAC sensors to the gripper of a PR2 robot and had it perform exploratory procedures with various household objects, using multimodal sensor feedback to assign haptic adjectives [20]. Mittendorfer et al. used their multimodal tactile sensing skin system on an HRP-2 robot to aid in whole-body grasping, but did not focus on force and thermal sensing [31]. Similarly Maiolino et al. tested their device on a number of robotic platforms but focused on force sensing, using thermal sensing primarily for temperature compensation [28].

In contrast to these studies, we evaluated our skin for use by a robot to recognize materials and recognize contact with humans. Due to the complexity of robotic skin, robotic manipulation, and the human body, it is difficult to predict how well a new skin design will perform when actually being used by a robot. Consequently, we conducted our tests with a real robot performing two manipulation tasks and making contact with people at two

locations on their bodies. Our evaluation provides evidence that our skin design could be beneficial for robots operating in human environments. This also goes beyond our previous work in this area [3], which only used data collected with a handheld device operated by people.

CHAPTER 3

DEVICE DESCRIPTION

Fig. 3.1 shows our fabric-based force and thermal sensing skin prototype covering the end effector of a Meka M1 Mobile Manipulator. As shown in Fig. 3.2, the skin has 12 circumferential taxels (each of area $2.2\,\mathrm{cm}^2$) and 1 end taxel (area $3.8\,\mathrm{cm}^2$) for a total of 13. As seen in the figure each fabric-based force sensing taxel is separated by a $5\,\mathrm{mm}$ gap, bringing the overall sensing area to approximately $60\,\mathrm{cm}^2$. Note that because of the multiple layers of fabric that help to distribute pressure, contacts that occur in between two force sensing taxels are still detected using the force sensors.

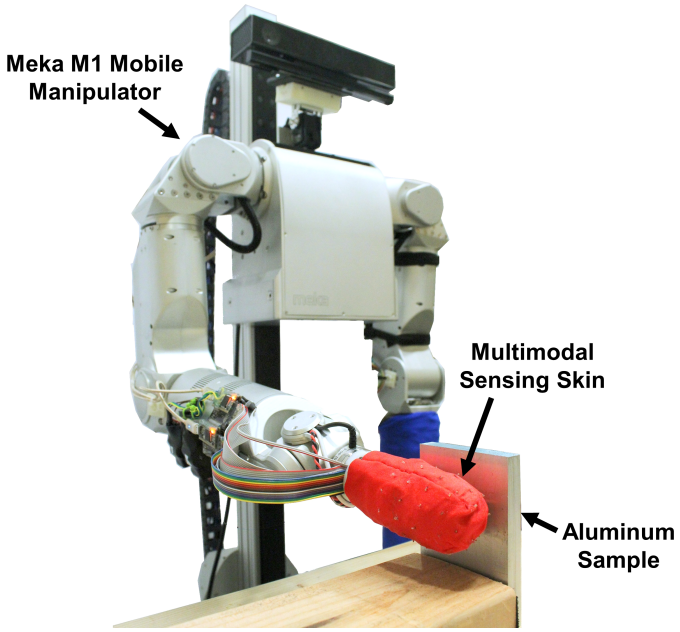

Figure 3.1: *Multimodal skin prototype attached to the end effector of a Meka M1 Mobile Manipulator.*

As shown in Fig. 3.3 and Fig. 3.5, each taxel features a fabric-based force sensor and four thermistors divided into two groups. In this work we use group 1 for active thermal sensing and group 2 for passive thermal sensing. Thus the entire skin has $13 \times 2 = 26$ active

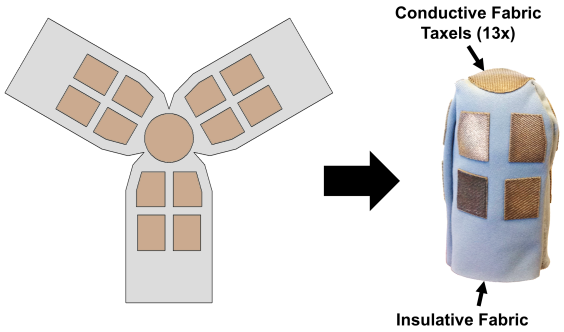

Figure 3.2: *Arrangement of force sensing taxels on our multimodal skin prototype.*

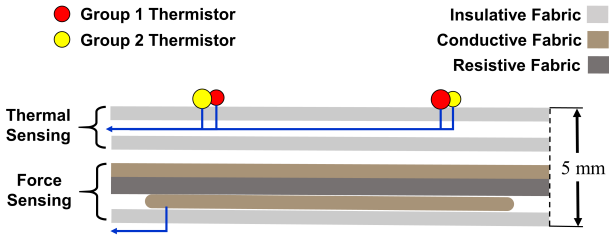

Figure 3.3: *Multimodal taxel design.*

thermal sensors and 26 passive thermal sensors.

3.1 Fabric-Based Force Sensors

Each force sensor is composed of a layer of Eeonyx LG-SL-PA-20K stretchable resistive fabric between two layers of LessEMF stretchable conductive fabric (silver plated 76% nylon, 24% elastic fiber) based on the design in [4].

Fig. 3.4 shows a schematic of the voltage divider circuit used to measure the resistance, R_{F}, of each fabric-based force sensitive resistor (FSR). In our previous work, we calibrated the fabric-based force sensor using an ATI Nano25 Force/Torque sensor and found that its voltage-to-normal force relationship can be approximated given the contact area using a 3rd order polynomial fit for forces up to $70\,\mathrm{N}$ [4]. Because the interaction forces used in this study were $< 15\,\mathrm{N}$, we used a voltage divider reference resistor, $R_{\mathrm{ref}} = 1\,\mathrm{k}\Omega$ to increase the sensitivity for forces in this range. Also, because the taxels used in this skin design were comparatively small compared to the touched objects, we assumed the contact area would be the same size as the taxel. For this range of forces, we found that our previous 3rd order

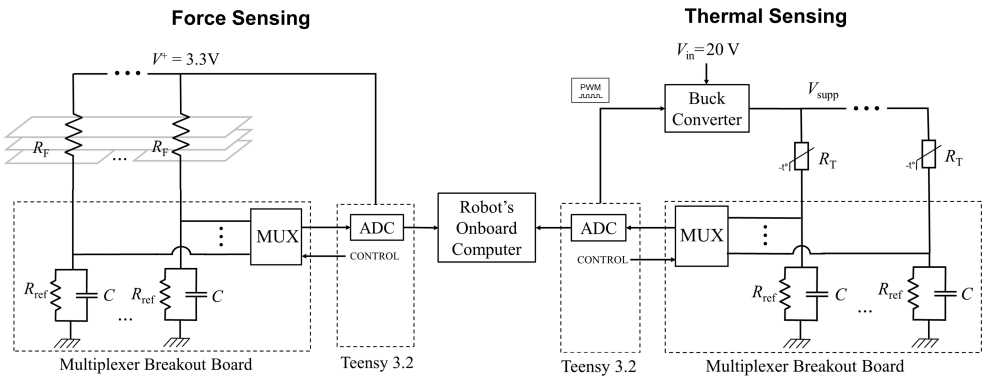

Figure 3.4: *Schematic of force and thermal sensing circuits.*

polynomial fit is approximately linear [4]. Based on this, we mapped the output voltage to force in Newtons using a linear fit.

3.2 Active and Passive Thermal Sensors

As shown in Fig. 3.3, and Fig. 3.5 each multimodal taxel features four fast-response $10\,\text{k}\Omega$ thermistors [33] evenly distributed across the skin. Fig. 3.4 shows a schematic of the circuit used to provide power to, and measure the resistance of, each thermistor. The system then converts this resistance value to temperature in Celsius using calibration constants provided by the manufacturer. We implemented a digitally controlled buck converter [34] to provide a variable DC voltage, $3.3\,\text{V} \leq V_{\text{supp}} \leq 10.5\,\text{V}$, to each thermistor. If $V_{\text{supp}} = 3.3\,\text{V}$. the current flowing through the resistor and the resistive heating in the thermistor are small, allowing for passive thermal sensing. By increasing V_{supp} to $9\,\text{V}$, the interior of each thermistor self-heats to a temperature of $55\,^{\circ}\text{C}$ in a room at $25\,^{\circ}\text{C}$, allowing for active thermal sensing similar to [35] and [36]. This active thermal sensor initial temperature of $55\,^{\circ}\text{C}$ is higher than the setting used in our previous work in [3] and [37]. It allows for a larger response when the sensors make contact with a material and as discussed in Section 4.4, does not create a significant safety hazard. Under these conditions, the thermistors are within their recommended operating range in terms of power and temperature [33].

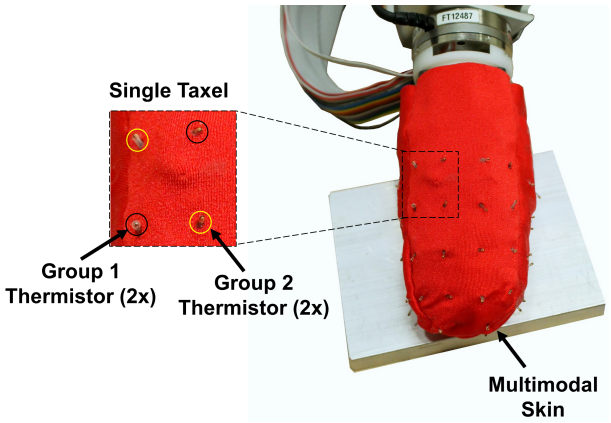

Figure 3.5: *Multimodal force and thermal sensing skin prototype.*

3.3 Active Thermal Temperature Controller

We defined two groups of thermistors using an alternating pattern as shown in Fig. 3.5 and powered each group of thermistors by an independent buck converter. Thus, each taxel included two thermistors in each group and the entire skin required two buck converters. In this work, we used the group 1 thermistors for active thermal sensing by initially setting V_{supp_1} to 9 V and then using a closed-loop integral controller to adjust V_{supp_1} to drive the mean temperature of the group 1 thermistors, $\bar{T}_1$, to the user-defined setpoint, $T_{\text{set}} = 55\,^{\circ}\text{C}$. The controller is described by

$$V_{\text{supp}_1}(t) = V_{\text{supp}_1}(0) - k_i \int_0^t \epsilon(t')dt' \tag{3.1}$$

where V_{supp_1} is constrained to be between 3.3 and 10.5 V. The error, $\epsilon(t)$, is given by

$$\epsilon(t) = \bar{T}_1 - T_{\text{set}} \tag{3.2}$$

While this controller helps ensure that the active thermal sensors are at the user-defined temperature setpoint prior to contact with the object, it is important that it does not respond so quickly that it cancels informative changes in temperature when the skin comes in contact with an object. To prevent this we used a low controller gain, $k_i = 5\,\text{mVK}^{-1}\text{s}^{-1}$. Thus if

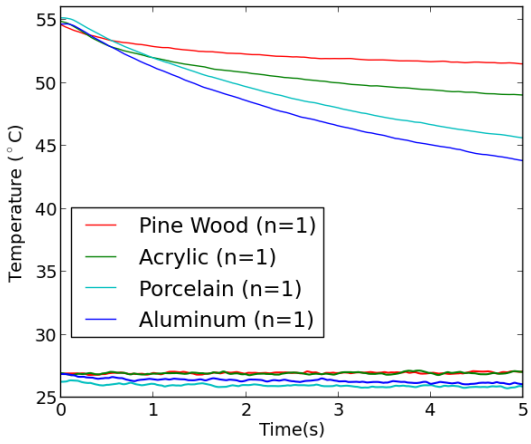

Figure 3.6: *Representative active and passive thermal sensor data resulting from touching the skin once each to four material samples. The data is filtered with a 2nd order low pass Butterworth filter with a cutoff frequency of 10 Hz.*

2 of the 26 active thermistors make contact with an object for 2.0 s and their temperature immediately drops by $5\,^{\circ}\mathrm{C}$, the mean active temperature will decrease by only $0.4\,^{\circ}\mathrm{C}$, and V_{supp_1} will change by only $4\,\mathrm{mV}$ based on the integral controller described in (3.1). In the extreme case, if many active thermistors contact a cold surface for a long period of time, the controller will adjust V_{supp_1} to the maximum voltage at $10.5\,\mathrm{V}$ but will not increase further.

While this control method effectively regulated the mean active thermistor temperature to $55\,^{\circ}\mathrm{C}$, the temperature of individual active thermistors varied by up to $\pm 2\,^{\circ}\mathrm{C}$ while the robot held the skin in air. This was likely due to slightly different heat transfer rates between the individual active sensors and the fabric to which they were mounted as shown in Fig. 3.5. One way to account for this variation in our system could be to use individual closed-loop controllers on each active thermistor. However, this would require many individually-controlled DC voltage sources and makes scaling to larger areas more difficult.

We used the group 2 thermistors for passive thermal sensing by setting V_{supp_2} to a constant $3.3\,\mathrm{V}$. Fig. 3.6 shows representative active and passive thermal sensor data collected from touching the skin to four material samples. Note that the approximate $\pm 0.5\,^{\circ}\mathrm{C}$ variation in initial passive sensor temperature is due to the fluctuations in the temperature of the room.

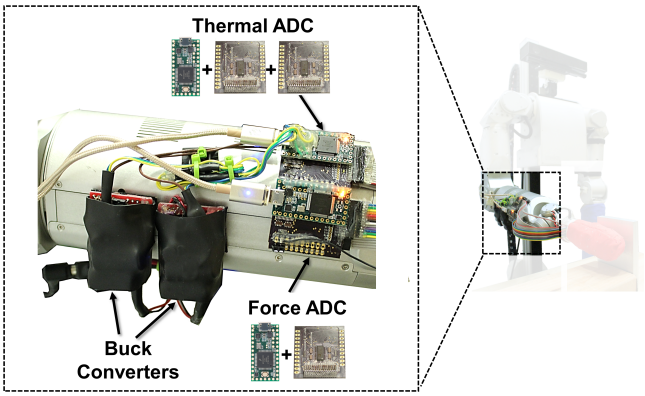

Figure 3.7: *Electrical hardware for multimodal skin: Teensy 3.2's and custom multiplexer breakout boards for analog-to-digital conversion (ADC) and buck converters for active thermal sensing.*

3.4 Power and Analog-to-Digital Conversion

Fig. 3.7 shows the hardware used to power the skin and perform analog-to-digital conversion (ADC). In contrast to skin systems with fully-integrated circuitry [28], [29], [30], the buck converters and ADC hardware used in this prototype are separate from the skin and are mounted to the robot's forearm. Though it increases the overall form factor of the system, this approach is advantageous in that most of the circuitry is separate from the skin and helps to maintain the flexibility and stretchability of the fabric-based skin. Note that while the thermistor connecting wires are not stretchable, they are designed to be longer than necessary to accommodate stretching in the fabric.

We selected the Teensy 3.2 microcontroller [38] based on its compact size and fast processor speed and used its built-in ADCs to read data from the skin with 12-bit resolution. Each Teensy 3.2 reads data and sends it to the robot's onboard computer via USB at 100 Hz.

While both our force and temperature modalities rely on resistive sensing and use identical circuitry for analog-to-digital conversion, we found that the larger magnitude analog signals resulting from the force sensors can affect the signal readings from the more sensitive thermistors. To prevent this, we separated our ADC circuitry: using one Teensy 3.2 and one multiplexer board to measure the 13 fabric-based force sensors and a second

Table 3.1: Estimated power and bandwidth requirements for larger scale skins.

# Taxels	Area (cm^2)	Analog Channels	Power (W)	Bandwidth (kbits/s)
13	**60**	**65**	**0.38**	**78**
20	92	100	0.58	120
40	185	200	1.12	240
80	370	400	2.32	480

Teensy 3.2 and two multiplexer boards to read data from the 52 thermistors (note that each taxel consists of one force sensor and four thermistors).

To accommodate the analog channels, we designed a custom breakout board to hold two 16 channel ADG1606BRUZ multiplexers (one on each side). Because the multiplexer selection ports are connected in parallel to the microcontroller, up to 10 multiplexer breakout boards can be connected to a single Teensy 3.2 using 20 of of its 21 analog input pins. Thus, the system can be scaled up to 320 analog input channels per microcontroller for larger-scale skin designs. So, we would expect two microcontrollers to support up to 80 taxels. In this arrangement, the microcontroller measuring thermal sensor data would have 320 analog channels while the microcontroller measuring the force sensors would have 80.

As shown in Fig. 3.4, the multiplexer breakout board includes a voltage divider circuit for each channel with reference resistors $R_{\mathrm{ref}} = 1\,\mathrm{k}\Omega$. With this reference resistor, each force sensing taxel requires up to 10 mW of power during normal operation. With the active thermal sensors controlled at $55\,^{\circ}\mathrm{C}$, each thermistor requires approximately $18\,\mathrm{mW}$ of power, whereas the passive sensors each require approximately 1 mW. Based on this, the 13 taxel prototype we present uses up to $380\,\mathrm{mW}$ of power total or $29\,\mathrm{mW}$ per taxel. Table 3.1 outlines the estimated power and bandwidth requirements for larger-scale skins designs.

We added a capacitor in parallel to each reference resistor to filter noise. Nominally a large capacitor would be used to specify a lowpass filter cutoff frequency less than the Nyquist frequency of our ADC to prevent aliasing. However, because each thermistor

requires an individual filtering capacitor and the noise occurs primarily at frequencies greater than $10\,\mathrm{kHz}$ we chose a smaller element ($C = 0.022\,\mu\mathrm{F}$) that helped filter this noise but did not significantly increase the form factor of each multiplexer board.

CHAPTER 4
HARDWARE ANALYSIS

4.1 Model of Thermal Sensor Distribution

Because the thermal sensors used in this design are small in size, it is difficult to cover a large area of the robot while keeping the overall system scalable. To address this, we developed a geometric model to guide the sparse distribution of thermal sensors across an area of the robot to maximize the chance of contact while minimizing the total number of sensors. We used this design in our skin because in human environments flat rigid surfaces and compliant low-curvature objects (including the human body) are common. Our use of sparsely-distributed thermal sensors and tactile sensors with low spatial resolution has some parallels to the variation in tactile modalities and effective spatial resolution across different parts of the bodies of biological organisms. For example, human skin can perform tactile sensing with much higher spatial resolution at the tip of the finger than across the torso [39].

In contrast to thermal sensor array designs such as [26], where high resolution sensors were used to create a thermal image, we designed the placement of our thermal sensors so that a single sensor from each group would make contact when the skin touches a material and therein infer information about the temperature and thermal effusivity of the touched object. This approach decreases the number of thermal sensors required and improves scalability for larger-area tactile sensing skins.

Because the skin's thermal sensors use thermistors of small cross-sectional area ($0.015\,\mathrm{cm}^2$) compared to our force sensing taxels ($2.2\,\mathrm{cm}^2$), we model them as point sensors. Note that this modeling approach differs from work with non point-like sensors including [40]. To determine the distribution of point sensors along the circumference and axis of the skin covering the robot's cylindrical end effector, we developed a planar geometric model of the

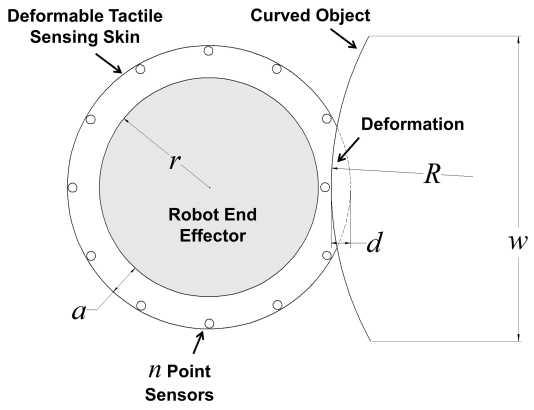

Figure 4.1: *Model used to determine number of circumferential thermal sensors.*

number of point sensors that will make contact with a curved object.

To determine the appropriate number of circumferential taxels to cover the robot's cylindrical end effector shown in Fig. 3.1 and Fig. 3.5, we used our planar model to predict the number of point sensors that will make contact when the cylinder touches the center of an object with a radius of curvature R and width w. Fig. 4.1 shows the robot's rigid cylindrical end effector of radius r covered with the deformable tactile sensing skin of thickness a. During contact, the skin compresses a distance d with a small applied force.

This circumferential model yields

$$n = \left\lceil \frac{k_c \pi}{\cos^{-1}\left(\frac{-d^2+2d(r+a)+2dR-2(r+a)^2-2R(r+a)}{2(r+a)(d-r-a-R)}\right)} \right\rceil \tag{4.1}$$

provided that

$$w \geq 2(r+a)\sin\frac{k_c \pi}{n} \tag{4.2}$$

where n is the required number of point sensors evenly spaced around the circumference of the skin for at least k_c point sensors to make contact with the surface. Appendix A provides a detailed derivation of (4.1).

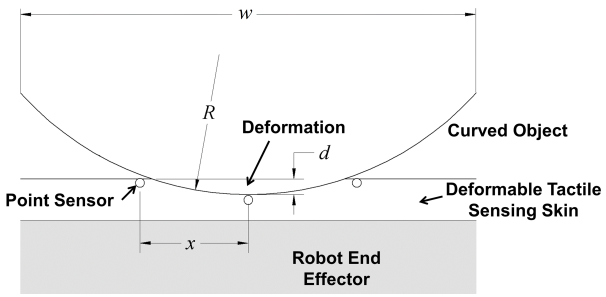

Figure 4.2: *Model used to determine thermal sensor spacing along cylinder axis.*

For the case where the skin touches a flat object ($R = \infty$), the model reduces to

$$n_{R=\infty} = \left\lceil \frac{k_c \pi}{\cos^{-1}\left(1 - \frac{d}{r+a}\right)} \right\rceil \tag{4.3}$$

For our prototype, $r = 17\,\text{mm}$, $a = 5\,\text{mm}$, $d = 3\,\text{mm}$. Because the thermistors are grouped in an alternating pattern, we designed our skin to achieve $k_c = 2$ for flat surfaces to ensure that at least one thermistor from each group will make contact. This implies $n = 12$ thermistors in the circumferential direction which motivated our choice of 6 circumferential taxels as shown in Fig. 3.2. With this number of taxels, contact with a single thermistor of either group ($k_c = 1$) is guaranteed based on this model when the surface's radius is of curvature $R \geq 8.5\,\text{mm}$. For objects with a radius of curvature $R < 8.5\,\text{mm}$, contact with a thermistor may not occur, though the skin's fabric-based force sensors should still detect the contact.

As shown in Fig. 4.2, we also applied our planar model to the number of point sensors along the axis of the robot's cylindrical end effector that will make contact with a curved sample.

Based on this model we found the required spacing, x, between each point sensor to be

$$x = \frac{2\sqrt{2dR - d^2}}{k_c} \tag{4.4}$$

provided that

$$w \geq k_c x \tag{4.5}$$

For our prototype, we chose $x = 17\,\mathrm{mm}$ which corresponds to $R = 50\,\mathrm{mm}$.

4.2 Thermal Sensor Noise Analysis

In order to characterize the noise in our active and passive thermal sensors, we used an oscilloscope to measure the output voltage from the thermistors in air and the output of the buck converter that supplies power to the thermistors (V_{supp}). The predominant noise occurred at 125 kHz, which is 4 times the PWM frequency used to control the buck converters (31.25 kHz). We measured the PWM signals from the Teensy 3.2 and found that the nominally square wave at 31.25 kHz had noise that occurred at 125 kHz. This noise in the PWM signals, and to a lesser extent the square waves themselves, led to noise in the output of the buck converters which then causes noise in the temperature readings.

To determine the noise level in units of temperature, we used the oscilloscope to measure the root-mean-square (RMS) of the thermistor voltage output and found this to be $\pm 9\,\mathrm{mV}$ for the active sensors ($V_{\mathrm{supp}_1} = 9\,\mathrm{V}$) and $\pm 8\,\mathrm{mV}$ for the passive sensors ($V_{\mathrm{supp}_2} = 3.3\,\mathrm{V}$). While the noise produced by the buck converters increases slightly as V_{supp} increases, the corresponding signal to noise ratio goes down. By converting this noise level to temperature, we found that the noise level for our active thermal sensors was $\pm 0.16\,^{\circ}\mathrm{C}$ and for the passive thermal sensors the noise level was $\pm 0.78\,^{\circ}\mathrm{C}$. To reduce this noise, we implemented a 2nd order low pass Butterworth filter with a cutoff frequency of 10 Hz in software to filter the thermistor data in real time. This filter design successfully reduced the noise without adding a significant delay in the signal.

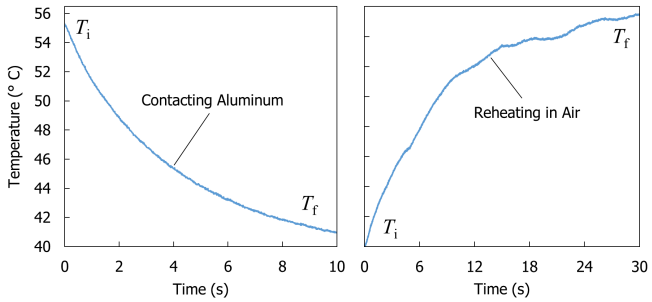

Figure 4.3: *Active thermal sensor touching aluminum (left) and active thermal sensor reheating in air (right).*

4.3 Active Thermal Sensor Time Response

To gain insight into the time response of the active thermal sensors while in contact with an object and compare our sensors to those used by other researchers, we employed a lumped capacitance model to consider the change in temperature as an exponential decay with associated time constant. This model assumes that the body of the thermistor is at a uniform temperature at each point in time, and the heat transfer from the thermistor to the object is proportional to the temperature difference. Based on these assumptions, the heat transfer from the thermistor to the object can be modeled as thermal capacitor discharging through a thermal resistor [41]. It follows that the thermistor temperature, $T(t)$ will decay exponentially in the form

$$T(t) = T_{\mathrm{f}} + (T_{\mathrm{i}} - T_{\mathrm{f}})e^{-\frac{t}{\tau}} \tag{4.6}$$

where T_{i} and T_{f} are the initial and final temperatures. Note that due to heat generation in the thermistor, T_{f} will be greater than the object's temperature. To perform the analysis we first had the robot press a $15\,\mathrm{mm}$ thick room temperature sample of aluminum for $10\,\mathrm{s}$ and recorded the temperature as it decreased from $55\,^{\circ}\mathrm{C}$ during contact. Fig. 4.3 shows the data we used for the time constant analysis. By rearranging and taking the natural logarithm of

both sides of (4.6), we have

$$\ln\left(\frac{T(t)-T_{\mathrm{f}}}{T_{\mathrm{i}}-T_{\mathrm{f}}}\right)=-\frac{t}{\tau} \tag{4.7}$$

Through linear regression we obtained $\tau = 4.2\,\mathrm{s}$ and $R^2 = 0.998$.

To understand the time required for an active sensor to reheat following contact, we had the robot touch the aluminum sample then break contact and used the same linear regression method above, to find the average time constant during reheating to be $3.6\,\mathrm{s}$ ($R^2 = 0.997$). Thus, if the temperature of an active thermistor decreases from $55\,^{\circ}\mathrm{C}$ to $50\,^{\circ}\mathrm{C}$ from touching aluminum for 2.0 s, we can expect the thermistor to exhibit a 90% reheat time of 2.3 time constants or 8.3 s.

This simplified model of the heat transfer provides insight into how the sensor design affects the speed of response during active thermal sensing. Based on this model, the time constant, τ, is

$$\tau = R_{\mathrm{th}}C_{\mathrm{th}} \tag{4.8}$$

where R_{th} is the equivalent thermal resistance and C_{th} is the equivalent thermal capacitance of the thermistor [41].

Because the time constant of an active thermal sensor is proportional to the thermal capacitance of the sensor, decreasing this value can improve the speed of response. This is beneficial in two ways. When brought in contact with an object the sensor will respond more rapidly, potentially improving the speed at which a material can be recognized. Additionally, following contact, a lower thermal capacitance may allow the sensor to reheat more quickly with the same heating power. Often this is achieved by choosing a sensor of smaller size, but this can make the sensor more fragile, requiring a more durable and potentially less flexible substrate to protect it as seen in [24].

A second factor that can increase the time constant of the heat transfer from the thermistor

Table 4.1: Comparison of observed cooling time constants while touching aluminum with various active thermal sensors.

First Author	Year	Device Type	Thermal Sensing Method	Time Constant (s)
Engel [24]	2005	Array/skin	Custom 50 nm thick nickel RTDs	0.080
Monkman [15]	1993	Sensor	Pyrometer	0.260
Caldwell [14]	1993	Sensor	Peltier effect sensor	1.2
Russell [12]	1988	Array/skin	Thermistors embedded in surface of silicone	2.5
Yuji [23]	2000	Sensor	Pressure-conductive rubber used as thermistor	3.0
Monkman [15]	1993	Sensor	Peltier heat pump	3.4
Our approach	**2017**	**Array/skin**	**Thermistors on fabric surface**	**4.2**
Russell [13]	1985	Sensor	Thermistor embedded in surface of silicone	5.9
Takamuku [42]	2008	Sensor	Thermistors embedded in polyurethane	9.0
Siegel [27]	1986	Array/skin	Thermistors covered by silicone	10*
Lin [19]	2009	Sensor	Thermistor inside fluid-filled polymeric finger (BioTAC)	41

*Results with aluminum not reported; 10 s time constant observed with steel.

to a material and decrease the speed of response is thermal contact resistance between the thermistor and the object which can affect R_{th}. Like many standard thermistors, ours are approximately spherical [33]. Thus a small contact area is expected during contact with a rigid surface. This may increase the observed time constant associated with our active thermal sensors.

Table 4.1 compares various active thermal sensors based on their cooling time constant achieved while touching aluminum. As seen in the table, our approach yields faster results than the BioTAC sensor, but time constants as fast as 80 ms have been reported using custom 50 nm thick nickel RTDs on a polyimide skin [24].

4.4 Active Thermal Sensor Safety Analysis

In order to assess the safety of our robot skin being in contact with human skin, we modeled the temperature of human skin upon contact with a thermistor using a standard heat transfer

Table 4.2: Tabulated thermal effusivity values.

Material	Thermal Effusivity ($\mathrm{J\,m^{-2}K^{-1}s^{-0.5}}$)		
	Min	Max	Mean
Pine Wood [43]	331	506	419
Acrylic [43]	380	702	541
Porcelain [43]	1160	1330	1250
Aluminum [43]	13400	24000	18700
Human Skin [44]	1060	1420	1180
Glass [43]	1290	1550	1420

model with semi-infinite solids [11]. With the human skin at an initial temperature of $31\,^{\circ}\mathrm{C}$ and the thermistor at an initial temperature of $55\,^{\circ}\mathrm{C}$, upon initial contact we would expect the surface of the human skin where it contacts the heated thermistor to warm to approximately $44\,^{\circ}\mathrm{C}$. We modeled the human skin and glass thermistor as having thermal effusivities equal to their tabulated mean values in Table 4.2. Note that the thermistors are made of multiple materials encased in a glass bead but we assumed their thermal properties are that of glass.

Studies of thermal injury suggest that a surface temperature of $44\,^{\circ}\mathrm{C}$ would need to be maintained for greater than 5 hours to result in even minor injury to human skin [45]. In contrast, contact between human skin and a thermistor on our robot's skin results in a rapid drop in the thermistor's internal temperature, attaining a temperature of approximately $46\,^{\circ}\mathrm{C}$ in $2\,\mathrm{s}$ which would reduce the temperature of the human skin surface to $39\,^{\circ}\mathrm{C}$.

In [46] Ungar et al. at the NASA Johnson Space Center establish safe object temperature limits, based on the object's thermal effusivity, for contact with human skin for varying lengths of time. Using this approach, a glass object at $55\,^{\circ}\mathrm{C}$ can indefinitely contact human skin without injury. In addition, we have been unable to perceive the thermistors as being warm or hot when touched. Similarly, no participants in our study detailed in Section 5.2 made note of any discomfort or warmth from the robot's skin.

CHAPTER 5
EVALUATION OF THE SKIN

To evaluate the performance of the overall system, we conducted two experiments during which we had the robot perform manipulation tasks with the skin and analyzed the resulting sensor data based on how well it enabled material recognition. First, we had the robot perform pressing and sliding manipulation tasks with samples of four materials. Second, we had the robot move to make contact with one clothed and one unclothed body location on human participants to evaluate the system's performance in detecting contact with people. A video of the experimental procedure is available at youtu.be/IxANBLU-4TA.

5.1 Object Manipulation Experiments

Fig. 5.1 shows the experimental procedure we used to evaluate the skin's performance. Our objective was to distinguish between four materials during tasks representative of human environments [47]: pressing a stationary object and sliding an object across a table. We performed each task with 10 samples each of pine wood, acrylic, porcelain and aluminum. We chose these materials because they represent four common materials in homes with distinct thermal effusivities as shown in Table 4.2. In the first task, we programmed the robot to compliantly press the skin to the material sample for 2.0 s as shown in Fig. 5.1. After each trial the robot waited 60 s to allow the experimenter to change the material sample to another of equal thickness and then repeated the motion.

In the second task we attached the sample to a wooden block of mass $0.5\,\mathrm{kg}$ and added $1\,\mathrm{kg}$ of weights to increase the total mass to 1.5 kg. Using equilibrium point control, we programmed the robot to push and slide the block a distance of $20\,\mathrm{cm}$ in approximately 2.0 s as shown in Fig. 5.1. Similarly to the pressing task, we waited 60 s between each trial and tested once with each sample.

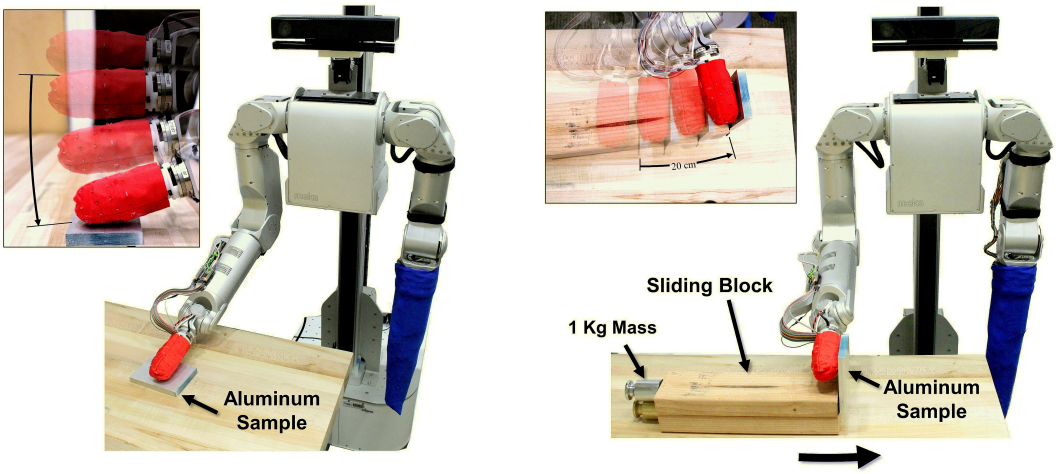

Figure 5.1: *Pressing task (left) and sliding task (right) used to evaluate the skin's performance.*

5.2 Experiments Contacting the Human Body

For the experiments with human participants, we recruited 10 people via word of mouth and obtained informed consent from each participant (3 female, 7 male from 18 to 23 years of age). Our study was approved by the Institutional Review Board of the Georgia Institute of Technology.

As shown in Fig. 5.2, each participant sat in a chair while the robot compliantly moved and made contact with two locations on the person's body, similar to the pressing task described in Section 5.1. We first asked the participant to rest their arm on table and, if necessary, roll up their sleeve so that their forearm was visible. We chose this location because in most cases, this area is either not covered by clothing or can be easily uncovered by rolling up the sleeve if necessary. We then had the robot move and gently make contact with the person's bare forearm for 2.0 s as shown in Fig. 5.2. To study the performance of our method in recognizing the human body through a layer of clothing, we had the robot make contact with the participant's shoulder for 2.0 s while it was covered by the sleeve of the participant's clothing (see Fig. 5.2). In this work we analyzed data resulting from one trial with each body location on each of our 10 participants.

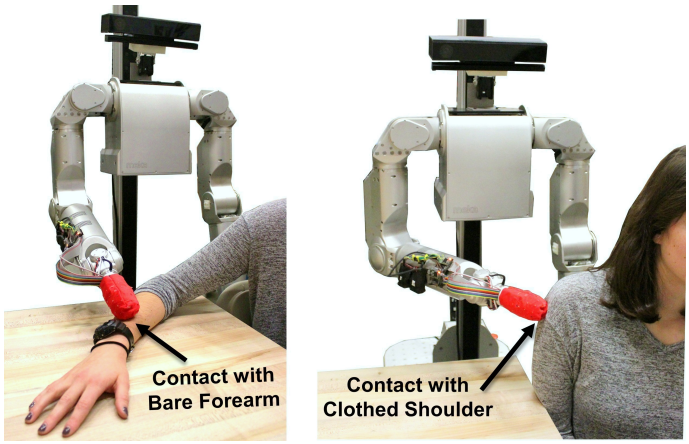

Figure 5.2: *Robot pressing bare forearm (left) and clothed shoulder (right) during experiments with human participants.*

5.3 Data Collection

We performed both experiments in a room at a mean temperature of $27\,^{\circ}\mathrm{C}$. While the data were collected, the room temperature varied by up to $\pm 1\,^{\circ}\mathrm{C}$, as measured by the passive thermistors. We used the skin's force modality to detect contact with a threshold of $0.7\,\mathrm{N}$. We used this threshold to account for false positives in the force readings due to hysteresis. When the force measured by a taxel exceeded this threshold, we checked both active thermistors on that taxel to see if they exhibited a negative time derivative (estimated using a first order difference) of temperature for $2.0\,\mathrm{s}$. This temperature decrease served as evidence that they were in contact with the material sample or human body at a lower temperature. If this condition was met, we saved time series data from this active thermistor and the force data from the corresponding taxel. This check is necessary because the thermistors are essentially point sensors compared to the force sensing taxels. If an object with high enough curvature or small enough size touches the taxel, the force sensor will detect it, but the object may not make contact with a thermal sensor.

It can be difficult to confirm if a passive thermistor made contact with the object or participant's body if little to no temperature change occurs. For objects that do not generate heat this is expected because the air and the object tend to be at the same temperature. While

people tend to be warmer than the surrounding air due to heat generation in the human body, this difference depends on the environment and body location [48] as well as the type of clothing worn. To overcome this challenge, when an active thermistor was determined to be in contact with the material, we assumed that the adjacent passive thermistor in the same circumferential position on the same taxel was also in contact and saved this time series as well. This is a fair assumption because the objects used in this experiment were flat and the human body locations were compliant.

Fig. 5.3 shows a visualization of the mean and standard deviation of the data collected during the pressing task and the sliding task. As seen in the figure, the 10 trials with each material and body location resulted in more than 10 distinct time series because two or more active thermistors can simultaneously make contact. This can occur when either both active thermistors on a single taxel simultaneously contact the sample or when active thermistors across multiple taxels make contact. These results agree with our model presented in Section 4.1.

Because we used a single buck converter and closed-loop controller to heat all the active thermistors to $55\,^{\circ}\mathrm{C}$ using the mean temperature as feedback (see Section 3.2), the temperature of a single active thermistor just prior to contact can vary from this desired value although the mean temperature is as desired. Because this variation may be due to changing environmental factors such as a varying room temperature, it is important to account for it so as not to bias the final results. For example, if the room were slightly warmer when we collected data from the aluminum samples compared to the pine wood, the data-driven algorithm might recognize this pattern and spuriously obtain a higher recognition accuracy. To reduce the influence of this variation, we subtracted the difference between the initial value and mean temperature ($55\,^{\circ}\mathrm{C}$ for active sensors, $27\,^{\circ}\mathrm{C}$ for passive) from every value in the time series. Thus, our active and passive thermal sensor data for all time series starts from the mean temperatures of $55\,^{\circ}\mathrm{C}$ and $27\,^{\circ}\mathrm{C}$, respectively. Though it makes the classification problem more difficult, this correction helps reduce bias from these factors.

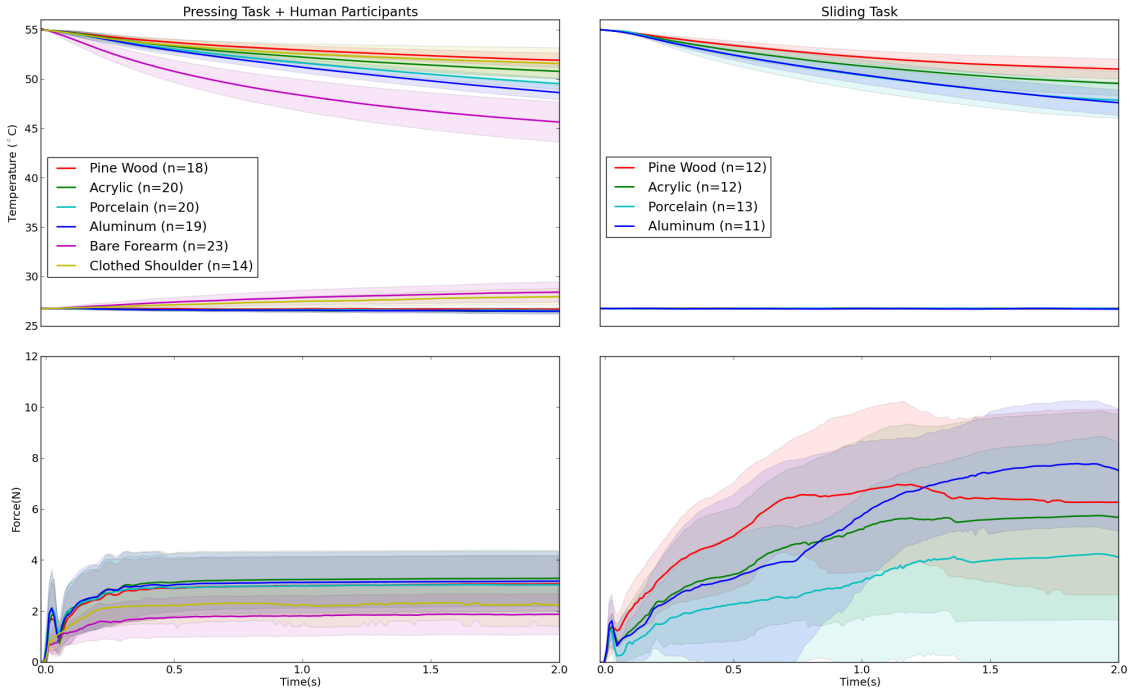

Figure 5.3: *Force and Thermal sensor data (mean ± standard deviation) recorded with 10 material samples each of pine wood, acrylic, porcelain and aluminum during pressing (left) and sliding tasks (right). The left graph includes data from contact with the bare forearm and clothed shoulder of 10 human participants. Note that the active and passive sensor data is biased to start from the mean temperatures of* $55\,^{\circ}\mathrm{C}$ *and* $27\,^{\circ}\mathrm{C}$*, respectively.*

5.4 Analyzing Skin Data

To evaluate the sensor data, we used a data-driven material recognition algorithm similar to our previous work in [11]. As discussed in Section 5.3, during each trial, multiple thermistors in the same group can make contact simultaneously. In our algorithm, we treat these multiple time series as independent feature vectors sampled from that material or body location. To study the effect of contact duration, we truncated the time series in time. We then took each temperature time series and concatenated it with its estimated time derivative to form a combined temperature and slope vector of twice the length as in [11]. For discrimination using only active or passive thermal sensing, this combined temperature and slope vector is the feature vector. For discrimination using multiple modalities, we concatenated the combined temperature and slope vectors from active and/or passive thermal sensing together

along with the vector of force data if used.

For classification, we implemented support vector machines (SVMs) using the scikit-learn package [49] in Python. We used a linear kernel and performed multiclass classification via pairwise coupling as described in [50]. To ensure that data collected from a single material sample or human participant were not simultaneously used for training and testing we used group 3-fold cross-validation.

5.5 Discriminating between Materials

As shown in Fig. 5.3, passive thermal sensing is not an effective sensing method for distinguishing materials that are at the ambient temperature. Similarly, because all material samples used have similar mass and relatively high moduli of elasticity, they cannot be easily distinguished using force sensing for the types of interactions we studied. For this reason, we performed material recognition using active thermal sensor data only. Tables 5.1 and 5.2 detail the multiclass and binary classification accuracy for the pressing and sliding tasks, respectively, with 0.25, 0.5, 1.0 and 2.0 s of contact. For cross validation we used group 3-fold cross-validation to train on data collected from a subset of the material samples and test on data collected from other samples.

Previous research by Ho and Jones suggests that humans can also have difficulty discriminating between two materials using active thermal sensing if the materials' thermal effusivities are similar. In their work human participants touched material samples for 10 s yet had difficulty distinguishing the samples if the ratio of the materials' thermal effusivities was less than three [51]. Based on this, we might expect humans to have difficulty distinguishing between pine wood and acrylic or acrylic and porcelain using only thermal cues because the ratio of their thermal effusivities is less than three.

As expected, the accuracy is higher for materials with more distinct thermal effusivities. As seen in Tables 5.1 and 5.2 our method distinguished pine wood from aluminum during the pressing task with 97% accuracy and in the sliding task with 92% accuracy with only

Table 5.1: Pressing task classification accuracy with active thermal sensors tested with different contact durations.

Classification Task	0.25 s	0.5 s	1.0 s	2.0 s
Multiclass (4 Materials)	43%	56%	62%	71%
Pine Wood vs. Aluminum	89%	97%	100%	100%
Acrylic vs. Aluminum	67%	97%	97%	100%
Porcelain vs. Aluminum	67%	69%	58%	77%
Pine Wood vs. Porcelain	84%	90%	97%	100%
Acrylic vs. Porcelain	59%	64%	88%	89%
Pine Wood vs. Acrylic	66%	61%	63%	69%
Average Binary Performance	72%	80%	84%	89%

Table 5.2: Sliding task classification accuracy with active thermal sensors tested with different contact durations.

Classification Task	0.25 s	0.5 s	1.0 s	2.0 s
Multiclass (4 Materials)	40%	31%	44%	88%
Pine Wood vs. Aluminum	79%	92%	88%	92%
Acrylic vs. Aluminum	58%	43%	70%	100%
Porcelain vs. Aluminum	61%	38%	49%	93%
Pine Wood vs. Porcelain	65%	57%	77%	93%
Acrylic vs. Porcelain	40%	60%	68%	93%
Pine Wood vs. Acrylic	67%	58%	71%	88%
Average Binary Performance	63%	58%	71%	93%

0.5 s of contact.

5.6 Recognizing Contact with the Human Body

To evaluate our skin's ability to recognize contact with people, we performed binary classification between the human body and the non-human material samples tested in the pressing task. Fig. 5.3 shows the skin's data used to perform classification. Note that the active thermal sensor temperature tends to decrease faster when contacting the bare forearm compared to aluminum even though aluminum has a higher thermal effusivity (see Table 4.2). This may be because the compliant human skin deforms around the spherical thermistor resulting in a larger contact area. This in turn allows for faster heat transfer.

Because the human body locations tested in this experiment are significantly more com-

Table 5.3: Human body classification accuracy with various combinations of active, passive and force sensing with 2.0 s of contact.

Classification Task	A	P	A+P	A+F	P+F	A+P+F
Human vs. Non-Human	81%	92%	93%	94%	93%	92%
Bare Forearm vs. Non-Human	98%	96%	98%	98%	99%	98%
Clothed Shoulder vs. Non-Human	82%	92%	92%	92%	93%	95%
Average Performance	84%	93%	94.3%	94.7%	95.0%	**95.0%**

*A=Active, P=Passive, F=Force

Table 5.4: Human body classification accuracy with combined active, passive and force sensing with different contact durations.

Classification Task	0.25 s	0.5 s	1.0 s	2.0 s
Human vs. Non-Human	83%	93%	91%	92%
Bare Forearm vs. Non-Human	91%	97%	97%	98%
Clothed Shoulder vs. Non-Human	85%	90%	88%	95%

pressible than the non-human material samples, force sensing provides further information by which they can be distinguished [47], [52], [8]. Additionally, passive thermal sensing can provide useful information in recognizing objects of elevated temperature such as the human body [3].

Table 5.3 details the classification accuracy using various combinations of force, active thermal and passive thermal sensing data. Note that discrimination using only force sensing is the focus of our previous work [47], [52], [8]. For the classification task we used the data from the skin to discriminate between all material samples tested in the pressing task versus the bare forearm only, the clothed shoulder only and combined forearm and shoulder (labeled 'Human'in the Tables 5.3 and 5.4). For cross validation we used group 3-fold stratified cross-validation to train on data collected from a subset of our human participants and test on data collected from other human participants and balance the data in the folds.

Our method exhibited the best performance discriminating between human vs. non-human using combined force and thermal sensing data from the skin, achieving 94% accuracy with force and active thermal sensing data and 93% accuracy with force and passive thermal with 2.0 s of contact. For detecting contact with the human body through a layer of clothing, our method achieved a maximum accuracy of 95% using combined force,

active and passive thermal sensing data. For recognizing the human body based on touching bare skin, we see that solely active or passive thermal sensing can achieve a high accuracy (98% and 99%, respectively). This may be because the compliance of the human skin allows for a greater contact area with the thermistor and faster heat transfer.

Table 5.4 outlines the binary classification accuracy based on all three of the skin's sensing modalities for discriminating between human and non-human with contact durations of 0.25, 0.5, 1.0 and 2.0 s. As seen in the table, longer duration contact can lead to more accurate results but our method successfully discriminated between contact with human and non-human with an accuracy of 93% using 0.5 s of contact.

CHAPTER 6
DISCUSSION AND LIMITATIONS

6.1 Skin Hardware

With the ADC hardware described in Section 3.4, the skin design can be scaled up to accommodate larger numbers of taxels, but because the ADC hardware and buck converters for the thermal sensors are external from the skin itself, extra space on the robot would be used. From a power standpoint this skin prototype used up to 29 mW of power per taxel which suggests that a scaled up version of the skin could place a non-negligible load on the robot's power supply.

For our skin design, all active thermistors share a common power supply (buck converter) and a single closed-loop controller regulates the average thermistor temperature at a user-defined setpoint prior to contact. While this method increases the scalability of the design by requiring only two buck converters, one for each thermistor group for an entire skin, this method also introduces drawbacks. Namely, a single controller for all thermistors allows for variability in the active thermal sensor temperature prior to contact.

To enhance contact, the thermistors are on the exterior of the skin and slightly protrude outward. This results in a skin surface that might be less suitable for some applications and could potentially catch on objects, such as when sliding along a surface. Moving the thermistors further back into the fabric and possibly covering them with a thin, thermally negligible material could potentially address these issues.

6.2 Skin Modeling

While the relatively sparse distribution of thermistors makes it possible for objects to touch the skin and not come into contact with any thermal sensors, this approach improves the

scalability of the overall system. Our geometric model presented in Section 4.1 accurately predicted that during contact with a flat surface, at least one active thermal sensor would touch the object. In our characterization of the active thermal sensor time response presented in Section 4.3, we found that the sensors exhibit a cooling time constant of 4.2 s. This relatively slow response time may be caused by the small contact area between the spherical thermistors and a flat surface. That said, as discussed in Chapter 5, reasonable inferences can be made based on the sensor data using as little as 0.5 s of data.

6.3 Skin Evaluation

Based on Section 5.5, for distinguishing between materials at room temperature based on their thermal properties, the skin's active thermal sensors showed success for enabling binary classification of materials with larger differences in thermal effusivities. However, the data from the skin was less informative for distinguishing materials of similar thermal effusivities.

As discussed in Section 5.6, the skin's force and active and passive thermal sensors enabled the most accurate recognition of contact with the human body. Though active or passive thermal sensing on their own may be effective at recognizing contact with a person's bare skin, our results suggests that the combination of force and active and passive thermal sensing is most informative for recognizing contact with the human body while it is covered in clothing.

CHAPTER 7
CONCLUSION

In this thesis, we presented the design of a fabric-based force and thermal sensing skin for robots in human environments. The skin features distributed self-heated thermistors for active and passive thermal sensing and fabric-based force sensors. After outlining the design of the skin, we analyzed the spacing of the thermistors used for thermal sensing using a geometric model and characterized the speed of response of the active thermal sensors using a simplified model of the heat transfer. Following this, we evaluated the skin by attaching it to the end effector of a Meka M1 Mobile Manipulator and used the robot to perform pressing and sliding tasks with 10 samples each of 4 materials. We also had the robot make contact with two locations on the arms of human participants. In our evaluation of the skin, we used the force modality to detect the onset of contact and implemented SVMs to discriminate between materials using active thermal sensing and recognize contact with the human body using force, active and passive thermal sensing. The skin enabled accurate discrimination between two materials with large differences in their thermal properties and in recognizing contact with people. This study demonstrates the feasibility of our fabric-based force and thermal sensing skin for robots. Our evaluation suggests that our multimodal tactile sensing skin can provide useful information to robots operating in human environments.

Appendices

APPENDIX A

DERIVATION OF CIRCUMFERENTIAL THERMISTOR SPACING MODEL

Figure A.1 shows the geometry used to derive the circumferential thermistor spacing model given by (4.1). The figure shows the case where $k_c = 1$: when the robot's cylindrical arm covered with the skin makes contact with a curved object of radius R, at least 1 circumferential thermistor will touch the object when the skin is compressed a distance $d = d_1 + d_2$.

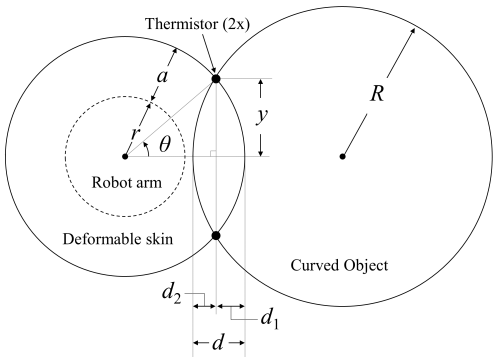

Figure A.1: *Geometry used to derive circumferential thermistor spacing model.*

Using the right triangle and angle θ shown in the figure,

$$d_1 = (r + a)(1 - \cos\theta) \tag{A.1}$$

furthermore, based on the Pythagorean theorem we can write

$$d_2 = R - \sqrt{R^2 - y^2} \tag{A.2}$$

Noting that

$$y = (r + a)\sin\theta \tag{A.3}$$

we can plug this into (A.2) to obtain

$$d_2 = R - \sqrt{R^2 - (r+a)^2 \sin^2 \theta} \tag{A.4}$$

Finally, note that if n thermistors are distributed uniformly around the circumference, their angular spacing will be 2θ, thus

$$n_{k_c=1} = \frac{2\pi}{2\theta} = \frac{\pi}{\theta} \tag{A.5}$$

Generalizing this to any value of k_c, we have

$$n = \frac{k_c \pi}{\theta} \tag{A.6}$$

and solving for θ,

$$\theta = \frac{k_c \pi}{n} \tag{A.7}$$

By plugging in this expression for θ into (A.1) and A.4, we can rewrite d as a function of n

$$d = (r+a)\left(1 - \cos\left(\frac{k_c \pi}{n}\right)\right) + R - \sqrt{R^2 - (r+a)^2 \sin^2\left(\frac{k_c \pi}{n}\right)} \tag{A.8}$$

We used Wolfram Alpha [53] to rearrange (A.8) to solve for θ and obtained

$$\theta = \cos^{-1}\left(\frac{-d^2 + 2d(r+a) + 2dR - 2(r+a)^2 - 2R(r+a)}{2(r+a)(d-r-a-R)}\right) \tag{A.9}$$

By plugging this result into (A.6) and noting that n must be a positive integer we obtain

the final result

$$n = \left\lceil \frac{k_c \pi}{\cos^{-1}\left(\frac{-d^2+2d(r+a)+2dR-2(r+a)^2-2R(r+a)}{2(r+a)(d-r-a-R)}\right)} \right\rceil \tag{A.10}$$

REFERENCES

[1] A. Jain, M. D. Killpack, A. Edsinger, and C. C. Kemp, "Reaching in clutter with whole-arm tactile sensing," *The International Journal of Robotics Research*, vol. 32, no. 4, pp. 458–482, 2013.

[2] P. M. Grice, M. D. Killpack, A. Jain, S. Vaish, J. Hawke, and C. C. Kemp, "Whole-arm tactile sensing for beneficial and acceptable contact during robotic assistance," pp. 1–8, 2013.

[3] T. Bhattacharjee, J. Wade, Y. Chitalia, and C. C. Kemp, "Data-driven thermal recognition of contact with people and objects," pp. 297–304, 2016.

[4] T. Bhattacharjee, A. Jain, S. Vaish, M. D. Killpack, and C. C. Kemp, "Tactile sensing over articulated joints with stretchable sensors," pp. 103–108, 2013.

[5] M. Cutkosky and W. Provancher, "Force and tactile sensors," in *Springer Handbook of Robotics*, Springer, 2016, ch. 28, pp. 717–736.

[6] A. Billard, A. Bonfiglio, G. Cannata, P. Cosseddu, T. Dahl, K. Dautenhahn, F. Mastrogiovanni, G. Metta, L. Natale, B. Robins, *et al.*, "The roboskin project: Challenges and results," in *Romansy 19–Robot Design, Dynamics and Control*, Springer, 2013, pp. 351–358.

[7] Y. Ohmura, Y. Kuniyoshi, and A. Nagakubo, "Conformable and scalable tactile sensor skin for curved surfaces," pp. 1348–1353, 2006.

[8] T. Bhattacharjee, J. M. Rehg, and C. C. Kemp, "Inferring object properties from incidental contact with a tactile sensing forearm," *ArXiv preprint arXiv:1409.4972*, 2014.

[9] G. Büscher, R. Kõiva, C. Schürmann, R. Haschke, and H. J. Ritter, "Flexible and stretchable fabric-based tactile sensor," in *IEEE/RSJ International Conference on Intelligent Robots and Systems (IROS 2012), Workshop on Advances in Tactile Sensing and Touch based Human-Robot Interaction*, Vilamoura, Algarve, Portugal, 2012.

[10] ——, "Tactile dataglove with fabric-based sensors," in *IEEE-RAS International Conference on Humanoid Robots (Humanoids 2012)*, Osaka, Japan, 2012.

[11] T. Bhattacharjee, J. Wade, and C. Kemp, "Material recognition from heat transfer given varying initial conditions and short-duration contact," 2015.

[12] R. A. Russell, "Thermal sensor for object shape and material constitution," *Robotica*, vol. 6, no. 01, pp. 31–34, 1988.

[13] R. A. Russell and F. J. Paoloni, "A robot sensor for measuring thermal properties of gripped objects," *Instrumentation and Measurement, IEEE Transactions on*, vol. 34, no. 3, pp. 458–460, 1985.

[14] D. G. Caldwell and J. O. Gray, "'dynamic'multi-functional tactile sensing," in *RoManSy 9*, Springer, 1993, pp. 187–198.

[15] G. J. Monkman and P. M. Taylor, "Thermal tactile sensing," *Robotics and Automation, IEEE Transactions on*, vol. 9, no. 3, pp. 313–318, 1993.

[16] R. Di Giacomo, L. Bonanomi, V. Costanza, B. Maresca, and C. Daraio, "Biomimetic temperature sensing layer for artificial skins," *ArXiv preprint arXiv:1512.01161*, 2015.

[17] D. Xu, G. E. Loeb, and J. A. Fishel, "Tactile identification of objects using bayesian exploration," pp. 3056–3061, 2013.

[18] E. Kerr, T. M. McGinnity, and S. Coleman, "Material classification based on thermal properties-a robot and human evaluation," pp. 1048–1053, 2013.

[19] C. H. Lin, T. W. Erickson, J. A. Fishel, N. Wettels, and G. E. Loeb, "Signal processing and fabrication of a biomimetic tactile sensor array with thermal, force and microvibration modalities," pp. 129–134, 2009.

[20] V. Chu, I. McMahon, L. Riano, C. G. McDonald, Q. He, J. Perez-Tejada, M. Arrigo, N. Fitter, J. C. Nappo, T. Darrell, and K. J. Kuchenbecker, "Using robotic exploratory procedures to learn the meaning of haptic adjectives," 2013.

[21] A. Gomez Eguiluz, I. Rano, S. Coleman, and M. McGinnity, "A multi-modal approach to continuous material identification through tactile sensing," 2016.

[22] D. Taddeucci, C. Laschi, R. Lazzarini, R Magni, P. Dario, and A. Starita, "An approach to integrated tactile perception," vol. 4, pp. 3100–3105, 1997.

[23] J. I. Yuji and K. Shida, "A new multifunctional tactile sensing technique by selective data processing," *Instrumentation and Measurement, IEEE Transactions on*, vol. 49, no. 5, pp. 1091–1094, 2000.

[24] J. Engel, J. Chen, Z. Fan, and C. Liu, "Polymer micromachined multimodal tactile sensors," *Sensors and Actuators A: Physical*, vol. 117, no. 1, pp. 50–61, 2005.

[25] J. Engel, N. Chen, C. Tucker, C. Liu, S. Kim, and D. Jones, "Flexible multimodal tactile sensing system for object identification," pp. 563–566, 2006.

[26] Y. J. Yang, M. Y. Cheng, S. C. Shih, X. H. Huang, C. M. Tsao, F. Y. Chang, and K. C. Fan, "A 32x32 temperature and tactile sensing array using pi-copper films," *The International Journal of Advanced Manufacturing Technology*, vol. 46, no. 9-12, pp. 945–956, 2010.

[27] D. Siegel, I. Garabieta, and J. M. Hollerbach, "An integrated tactile and thermal sensor," vol. 3, pp. 1286–1291, 1986.

[28] P. Maiolino, M. Maggiali, G. Cannata, G. Metta, and L. Natale, "A flexible and robust large scale capacitive tactile system for robots," *IEEE Sensors Journal*, vol. 13, no. 10, pp. 3910–3917, 2013.

[29] P. Mittendorfer and G. Cheng, "Humanoid multimodal tactile-sensing modules," *IEEE Transactions on robotics*, vol. 27, no. 3, pp. 401–410, 2011.

[30] ——, "Uniform cellular design of artificial robotic skin," pp. 1–5, 2012.

[31] ——, "Integrating discrete force cells into multi-modal artificial skin," pp. 847–852, 2012.

[32] F. Castelli, "An integrated tactile-thermal robot sensor with capacitive tactile array," vol. 3, pp. 1970–1975, 1995.

[33] *EPCOS (TDK) B57541G1103F NTC Thermistor 10k Bead, Glass*, `http://www.digikey.com/product-detail/en/epcos-tdk/B57541G1103F/495-4599-ND/3712554`. Accessed: 2017-03-10., 2016.

[34] *Variable 0-12V, Digitally Controlled, Power Supply using a Laptop Wall Wart & Ardunio*, `http://www.instructables.com/id/Variable-0-12V-Digitally-Controlled-Power-Supply-u`. Accessed: 2016-10-01, 2013.

[35] J. Valvano, J. Cochran, and K. Diller, "Thermal conductivity and diffusivity of biomaterials measured with self-heated thermistors," *International Journal of Thermophysics*, vol. 6, no. 3, pp. 301–311, 1985.

[36] H. Fujita, T. Ohhashi, M. Asakura, and K. Watanabe, "A thermistor anemometer for low flow rate measurements," pp. 1217–1220, 1994.

[37] J. Wade, T. Bhattacharjee, and C. C. Kemp, "Force and thermal sensing with a fabric-based skin," 2016.

[38] *Teensy 3.2*, https://www.sparkfun.com/products/13736. Accessed: 2017-03-10., 2016.

[39] S. Weinstein, "Tactile sensitivity of the phalanges," *Perceptual and motor skills*, vol. 14, no. 3, pp. 351–354, 1962.

[40] N. F. Lepora, U. Martinez-Hernandez, M. Evans, L. Natale, G. Metta, and T. J. Prescott, "Tactile superresolution and biomimetic hyperacuity," *IEEE Transactions on Robotics*, vol. 31, no. 3, pp. 605–618, 2015.

[41] T. L. Bergman, F. P. Incropera, D. P. DeWitt, and A. S. Lavine, *Fundamentals of heat and mass transfer*. John Wiley & Sons, 2011.

[42] S. Takamuku, T. Iwase, and K. Hosoda, "Robust material discrimination by a soft anthropomorphic finger with tactile and thermal sense," pp. 3977–3982, 2008.

[43] *CES EduPack database of natural and man-made materials*, Granta Design, 2016.

[44] *Tissue Properties*, http://www.itis.ethz.ch/itis-for-health/tissue-properties/database, 2016.

[45] A. R. Moritz and F. Henriques Jr, "Studies of thermal injury: Ii. the relative importance of time and surface temperature in the causation of cutaneous burns," *The American journal of pathology*, vol. 23, no. 5, p. 695, 1947.

[46] E. Ungar and K. Stroud, "A new approach to defining human touch temperature standards," vol. 6310, 2010.

[47] T. Bhattacharjee, J. M. Rehg, and C. C. Kemp, "Haptic classification and recognition of objects using a tactile sensing forearm," pp. 4090–4097, 2012.

[48] B. W. Olesen, "Thermal comfort," *Technical review*, vol. 2, pp. 3–37, 1982.

[49] F. Pedregosa, G. Varoquaux, A. Gramfort, V. Michel, B. Thirion, O. Grisel, M. Blondel, P. Prettenhofer, R. Weiss, V. Dubourg, J. Vanderplas, A. Passos, D. Cournapeau, M. Brucher, M. Perrot, and E. Duchesnay, "Scikit-learn: Machine learning in Python," *Journal of Machine Learning Research*, vol. 12, pp. 2825–2830, 2011.

[50] T.-F. Wu, C.-J. Lin, and R. C. Weng, "Probability estimates for multi-class classification by pairwise coupling," *The Journal of Machine Learning Research*, vol. 5, pp. 975–1005, 2004.

[51] H.-N. Ho and L. A. Jones, "Contribution of thermal cues to material discrimination and localization," *Attention, Perception, & Psychophysics*, vol. 68, no. 1, pp. 118–128, 2006.

[52] T. Bhattacharjee, A. Kapusta, J. M. Rehg, and C. C. Kemp, "Rapid categorization of object properties from incidental contact with a tactile sensing robot arm," 2013.

[53] *Wolfram Alpha LLC*. https://www.wolframalpha.com, 2009.